A comparison of infrared detection mechanisms in thermal-emissive vs. photo-emissive silicon Schottky barrier arrays

Freeman D. Shepherd and James E. Murguia
Solid State Scientific Corporation
27-2 Wright Road
Hollis, New Hampshire 03049

ABSTRACT

Infrared imaging based on photoemission in metal-silicide/silicon Schottky barrier arrays is a mature technology that is currently employed in both military and commercial applications. Metal-silicide/silicon Schottky diodes can also be employed in uncooled bolometer arrays. The bolometer detection mechanism is thermionic emission in the Schottky barrier. Schottky bolometer array technology is expected to have both performance and production advantages, when compared with current uncooled sensor technology. In this paper, we compare the physical mechanisms involved in the two Schottky barrier based infrared sensors. We will also present a simplified model for the noise equivalent temperature of each technology.

Keywords: Infrared imaging, Thermionic emission, Internal photoemission

1. INTRODUCTION

In 1973, Shepherd and Yang[1] proposed development of an infrared camera based on internal photoemission from silicon Schottky barrier arrays. Internal photoemission was known to be a low quantum efficiency process. However, it was expected that this problem could be overcome by operating in staring-mode, where the signal is accumulated over a video frame time, to improve signal to noise ratio. This technology, as typified by platinum silicide, operates in the near through medium wavelength infrared (MWIR) spectrum. Visible spectrum response can be obtained by "metal side" illumination.

Early staring-mode thermal imaging sensors were limited by spatial pattern noise, which obscured detail in the displayed image.[2] Pattern noise is caused by local photoresponse variations in the sensor focal plane.[3, 4] This effect is often called "fixed pattern noise"; however, detector 1/f-noise can cause drift in the configuration of the pattern. In order to realize pattern noise free imagery, staring-mode thermal imaging systems must be based on focal plane arrays having photoresponse uniformity of the order of 0.03 % rms. and low drift. This level of performance usually requires response compensation.

Pd_2Si/Si Schottky barrier internal emission detectors have extremely uniform photoresponse, when operated in reverse bias. Excellent uniformity is observed in scanning spot measurements of large detectors and between elements in detector arrays.[5] Similar uniformity is also found in arrays of Ni-, Co- and Pt-silicide/silicon photodiodes. Mooney has demonstrated that PtSi photodiodes operated under reverse bias have negligible 1/f-noise.[6]

In the mid 1970's Kohn and Schultz[7] and Kosonocky, et al[8], at the RCA Sarnoff Research Center, demonstrated infrared sensing IR-CCD arrays using both Pd_2Si and PtSi. The earliest 2-D CCDs had 1250 detectors in a 25 x 50 array. Ewing, Taylor, et al, at AFRL and Cantella and Klein at RCA incorporated Sarnoff arrays into infrared video cameras.[9] The AFRL cameras resolved 0.2 K image detail, without compensation, and better than 0.1 K, with offset compensation. The offset compensation frame was based on a 16-frame average of infrared background radiation.[10] The RCA and AFRL cameras were the first practical staring-mode, thermal imaging sensors.

Today there are monolithic PtSi focal planes with array size ranging from 480 x 640 to 1968 x 1968.[11] PtSi pixel sizes are in the 25 to 30 um range. There are also high fill factor, bump bonded, 256 x 256 and 240 x 320 PtSi arrays, which were developed for industrial cameras and radiometers. The best PtSi based cameras display pattern noise free imagery with background shot Noise Equivalent Temperature Differences (NETDs) near 60 mK, using only offset compensation.

The market for PtSi-based sensors is limited by the need for focal plane cooling, which adds to sensor cost and complexity. It is also limited by the low quantum efficiency, near 1%, and the spectral response roll off with wavelength observed in PtSi detectors. In addition, no practical PtSi, or other metal-silicide photo-emission detector, has been developed for imaging in

the long wavelength infrared (LWIR) spectrum, between 8 and 14 um. The LWIR band is preferred for many thermal imaging applications, because similar signals are obtained day and night.

Recently Murguia and Tedrow, et al,[12] demonstrated metal-silicide/silicon Schottky diodes can be employed in uncooled diode bolometer arrays, wherein, individual detectors are thermal isolated, using the same fabrication techniques currently employed in VO_x resistive bolometer arrays. When the image of an infrared scene is incident on a Schottky bolometer array, the temperature of individual detectors will be increased in proportion to the local image power. This will cause increases in thermionic emission from the array, resulting in the formation of an electronic "thermal" image of the scene.

Schottky bolometer arrays have a flat spectral response, which extends beyond the LWIR spectral band. The power absorption properties of Schottky bolometer detectors are equivalent to those of competing technologies. Schottky temperature coefficients, at 300K, are above 5%/K, more than double that of competing technologies. Schottky bolometer diode sensing elements retain the noise and procucibility advantages of PtSi technology. These devices are free of 1/f-noise. Pattern noise associated with the read-out multiplexer and with lithographic variation in the thermal isolation structure will be similar for all bolometer array technologies. Thus, Schottky bolometer arrays are expected to have both performance and production advantages, when compared with state of the art uncooled sensor technology.

2. THE INTERNAL EMISSION PROCESS

Internal emission describes the transit of an excited charge carrier, from a metal electrode into an adjoining semiconductor or dielectric. The charge carrier can be excited by a photon absorption event, or by scattering with a lattice vibration or an energetic carrier. The excited carrier must have energy equal to, or greater than, the energy of the Schottky barrier potential.

2.1. Internal Photoemission

During internal photoemission, carrier excitation is provided by the absorption of infrared photons in the metal electrode. The resulting emission into the adjacent semiconductor is the solid state analog of vacuum photoemission, as described by Fowler in the 1930's.[13] In vacuum photoemission, the electron emission spectrum increases with photon energy, from a threshold energy, corresponding to the work function of the metal. A similar spectrum is noted for internal photoemission, where the emission threshold corresponds to the potential of the Schottky barrier at the metal-semiconductor interface. Internal photoemission was first employed for accurate measurement of the barrier potential of metal-insulator and metal-semiconductor contacts. This work is reported by Crowell, et al,[14] and by Williams.[15]

The internal photoemission process involves three steps:

1) Free carrier photo-absorption in the Schottky electrode, giving rise to a hot carrier gas
2) Hot carrier transport in the electrode and in the semiconductor prior to the Schottky barrier peak.
3) Emission over the Schottky barrier.

Internal photoemission detectors have low quantum efficiency, the ratio of emitted electrons to incident photons. In addition, the photoemission efficiency rolls off with wavelength, to a cut off wavelength determined by the Schottky barrier potential, Φ_{bn}. Each of these characteristics is a direct result of conservation of carrier momentum, during the emission process. Momentum in the plane of the Schottky junction is conserved. Only momentum normal to the junction contributes to emission over the Schottky barrier and the emission process expends only normal momentum. Carriers directed away from the Schottky barrier and low energy carriers are not emitted. However, scattering can redirect energetic carriers toward the barrier, resulting in additional emission. Mooney and Silverman give a detailed description of this process.[16]

The quantum efficiency for photoemission $Y(h\nu)$ is given by the product of the detector photoabsorption efficiency and the excited electron emission efficiency, both of which may be photon energy dependent.

$$Y(h\nu) = A(h\nu)\ \eta_t(h\nu) \tag{2.1}$$

Where $h\nu$ is the photon energy and $A(h\nu)$ photoabsorption in the PtSi metal film. Throughout the current discussion we will assume $A(h\nu)$ is a constant unity multiplier. Actually $A(h\nu)$ varies with wavelength, electrode film thickness and electrode

geometric configuration. Details of this variation are given by Archer and Cohen[17] and by Mooney.[18] Under this assumption, the quantum efficiency for internal photoemission is given by:

$$Y = C_f(h\nu - \Phi_{ph})^2 / h\nu \quad (2.2)$$

Where, C_f is the Fowler emission coefficient and Φ_{ph} is the Schottky barrier potential as determined from photoemission measurements. The Fowler coefficient provides an energy independent measure of the internal photoemission efficiency. Typical values for C_f are near 0.3 eV^{-1}.

2.2. Thermionic Emission

The saturation current density of properly fabricated Schottky diodes is dominated by thermionic emission, given by the Richardson equation:

$$J_s = A_r T^2 \exp(-\Phi_{bn}/kT) \quad (2.3)$$

Where A_r is Richardson's constant, k is Boltzmann's constant, T the absolute temperature and Φ_{bn} the Schottky barrier potential. The value of Φ_{bn} is determined by an activation energy analysis of the variation of diode current with temperature. The Richardson constant for p-type silicon Schottky barriers is 30 amperes/cm^2/K^2.

The barrier potential determined from photo-response measurements is normally higher than that determined from analysis of dark current variation with temperature. During dark current measurements, the electron energy spectrum is near thermodynamic equilibrium. The barrier potential determined from analysis of dark current vs. temperature should be very representative of the actual junction potential. During photoresponse measurements, the initial photo-excited electron energy spectrum is hot compared to an equilibrium spectrum. This energy spectrum is partially cooled prior to emission, by transfer of energy to the crystal lattice through phonon scattering. The measured threshold energy for photoemission is increased by the energy lost to phonon scattering. The Schottky potentials for thermionic emission and photoemission will be related by:

$$\Phi_{ph} = nh\omega/2\pi + \Phi_{bn} \quad (2.4)$$

Where n is the average number of phonon scattering events and $h\omega/2\pi$ is the energy loss per event.

Consider the characteristics of the signals observed when Schottky diodes are used as infrared detectors. In the case of both photo detection and thermal detection, we measure changes in the emission current of a reverse biased Schottky diode. The diode has very high impedance and acts as a current source. The magnitude of the current will be proportional to the electrically active area of the Schottky junction. Otherwise, the two sensing mechanisms are quite different.

In the case of photo detection, the metal-silicide diode array is formed on a continuous silicon substrate. Silicon has a high thermal conductivity, which clamps the temperature of the array. Lithographic tolerances, or point defects, but not temperature differences, cause local dark current variations in the array. The signal is derived from the incident flux of "in band" photons, but the signal generation is energy dependent and weakly coupled. All photoelectrons originate in the metal-silicide electrode. Photons, which are absorbed outside of this electrode, are lost. The photo-excited electrons are a subset of the total number of electrons in the electrode. Electrons excited to energies below the barrier potential are blocked from emission. Scattering losses will also reduce emission. Finally, the number of emission electrons is reduced by conservation of momentum, during transit of the Schottky barrier. The observed current is de-coupled from the initial photo-excitation event by several loss mechanisms, resulting in low emission efficiency.

In the case of bolometer detection, each detector element is "thermally isolated" and is allowed to float in temperature. Power can be absorbed anywhere in the detector element. The change of the detector equilibrium temperature is determined by the power balance between radiation incident on the detector and power lost by radiation and conduction from the detector. The change in detector equilibrium temperature changes the total distribution of electron energies in the Schottky electrode, resulting in a change of the detector saturation current, following Equation 2.3. The detection process is a direct measure of the equilibrium temperature of the detector element. This process can be very efficient. The detector responsivity is determined by the thermal design of the detector element, including element absorption, thermal isolation and thermal capacitance. Responsivity will also be proportional to the electrical fill factor of the Schottky electrode.

3. DETECTOR THERMAL RESPONSE

In this development, we follow Murguia and Tedrow, et al.[19] Consider a pixel of area A_p and effective thermal detection area A_d, where:

$$A_d = A_p ff_{th} \tag{3.1}$$

Where ff_{th} is the detector thermal fill factor, determined by the amount of pixel area lost during thermal isolation of the detector element. The heat radiated from the surface of a detector at temperature T_d follows the Stefan-Boltzmann radiation law,

$$P_{rad} = A_d \varepsilon_d \sigma T_d^4 . \tag{3.2}$$

where ε_d is the detector emissivity and σ is the Stefan-Boltzmann constant. The thermal conductance of the detector due to radiation, G_{rad} is given by:

$$G_{rad} = 4A_d \varepsilon_d \sigma T_d^3 . \tag{3.3}$$

In Equation 3.3, the detector is approximated by a thin flat plate, which radiates in the forward direction. The radiation is assumed to be Lambertian.

The detector element will also lose heat by conduction to the focal plane substrate, which is clamped to the sensor enclosure temperature. We assume that the enclosure is at the background temperature, T_b. The conductive heat loss is:

$$P_{dif} = G_{dif}(T_d - T_b) \tag{3.4}$$

The optical power incident on the detector is the sum of the signal power and the background power.

$$P_d = P_{ds} + P_{db} = \frac{A_d \varepsilon_d \sigma T_s^4}{4F^2 + 1} + \left(1 - \frac{1}{4F^2 + 1}\right) A_d \varepsilon_d \sigma T_b^4 \tag{3.5}$$

In Equation 3.5, we have assumed that the signal is from an extended source, of unity emissivity, at temperature T_s.

The detector power balance in steady state is given by:

$$P_{rad} + P_{dif} = P_{ds} + P_{db} + I_d V_d \tag{3.6}$$

where I_d and V_d are the detector diode current and bias voltage. Except for a short read out interval, no bias is applied to the detector. Substituting from the above equations, the power balance becomes:

$$A_d \varepsilon_d \sigma T_d^4 + G_{dif}(T_d - T_b) = \frac{A_d \varepsilon_d \sigma T_s^4}{4F^2 + 1} + \left(1 - \frac{1}{4F^2 + 1}\right) A_d \varepsilon_d \sigma T_b^4 \tag{3.7}$$

Using a binomial expansion of Equation 3.7 about T_b, where:

$$T_d = T_b + \Delta T_d \tag{3.8}$$

and

$$T_s = T_b + \Delta T_s \tag{3.9}$$

Equation 3.7 can be approximated as:

$$\frac{4A_d \varepsilon_d \sigma T_b^3 \Delta T_s}{4F^2 + 1} = 4A_d \varepsilon_d \sigma T_b^3 \Delta T_d + G_{dif} \Delta T_d \tag{3.10}$$

Then substituting Equation 3.3 we have:

$$\Delta T_d = \left(\frac{1}{4F^2+1}\right)\frac{G_{rad}}{G_{rad}+G_{dif}}\Delta T_s \tag{3.11}$$

Equation 3.11 is valid for source temperatures near T_b, where the full blackbody spectrum of the source is transmitted to the detector. We can generalize Equation 3.11 to a wide range of source temperatures by defining a source contrast function based the variation of source emission with T_s^4 and the expansion of Equation 3.9:

$$\xi(\Delta T_s) = 6\left(\frac{\Delta T_s}{T_b}\right)^2 - 4\left(\frac{\Delta T_s}{T_b}\right)^3 + \left(\frac{\Delta T_s}{T_b}\right)^4 \tag{3.12}$$

Then :

$$\Delta T_d = \left(\frac{1}{4F^2+1}\right)\frac{G_{rad}(1+\xi(\Delta T_s))}{G_{rad}+G_{dif}}\Delta T_s \tag{3.13}$$

In the more general case, where the spectrum of the incident radiation is filtered, Equation 3.13 becomes:

$$\Delta T_d = \left(\frac{1}{4F^2+1}\right)\frac{G_{rad}(1+\xi(\Delta T_s))\Gamma(T_s,\lambda_1,\lambda_2)}{G_{rad}+G_{dif}}\Delta T_s \tag{3.14}$$

Where:

$$\Gamma(T_s,\lambda_1,\lambda_2) = \frac{\int_{\lambda_1}^{\lambda_2} W_\lambda(\lambda, T_s)d\lambda}{\sigma T_s^4} \tag{3.15}$$

and

$$W_\lambda(\lambda, T_s) = \frac{2\pi hc^2}{\lambda^5(\exp(\frac{hc}{\lambda k T_s})-1)} \tag{3.16}$$

where $W_\lambda(\lambda, T_s)$ is the spectral radiant emittance of the source at temperature T_s and c is the velocity of light.

Equation 3.14 gives the detector temperature change for thermal equilibrium. In a frame period, the response is reduced by:

$$R(\tau_{th}) = \left[1-\exp(\frac{-\tau_{th}}{t_{fr}})\right] \tag{3.17}$$

where t_{fr} is the sensor frame time and τ_{th} the detector thermal response time, with corresponding thermal bandwidth B_{th}.

$$\tau_{th} = \frac{C_{th}}{G_{th}} = \frac{1}{2B_{th}} \tag{3.18}$$

where G_{th} is the thermal conductance of the detector element

$$G_{th} = G_{rad} + G_{dif} \tag{3.19}$$

and C_{th} is the thermal capacitance.

$$C_{th} = A_d \rho c_d t_d \tag{3.20}$$

where t_d is the detector element thickness, ρ the mass density and c_d the specific heat of the detector structure.

The resulting change in detector temperature is given by:

$$\Delta T_d = \left(\frac{1}{4F^2+1}\right)\frac{G_{rad}(1+\xi(\Delta T_s))\Gamma(T_s,\lambda_1,\lambda_2)}{G_{rad}+G_{dif}}R(\tau_{th})\Delta T_s \quad (3.21)$$

We can express Equation 3.21 as a temperature transfer function, giving the change in detector temperature with the change in source temperature.

$$\Delta T_d = H(T_s)\Delta T_s \quad (3.22)$$

where:

$$H(T_s) = \left(\frac{1}{4F^2+1}\right)\frac{G_{rad}(1+\xi(\Delta T_s))\Gamma(T_s,\lambda_1,\lambda_2)}{G_{rad}+G_{dif}}R(\tau_{th}) \quad (3.23)$$

It can be seen, from Equation 3.23, that the detector thermal and electrical responses are separable

4. ELECTRICAL EQUATIONS

The current density in a Schottky diode based thermal detector is calculated from thermionic emission theory,[20]

$$J = J_s(e^{qV/kT}-1) \quad (4.1)$$

where J_s is the saturation current density, given by Equation 2.3. When the detector is operated under back bias, at voltages large compared to kT/q, the reverse diode current I_d reduces to the saturation current.

$$I_d = A_e J_s = A_e A_r T^2 e^{-q\Phi_{bn}/kT} \quad (4.2)$$

where A_e is the electrical active area of the detector, and Φ_{bn} the Schottky barrier potential for thermionic emission at V_d.

The change in the reverse current as a function of temperature, $\partial J_R/\partial T$, is given by:

$$\frac{\partial J_R}{\partial T} = T\left(\frac{q\Phi_{bn}}{kT}+2\right)A_r e^{-q\Phi_{bn}/kT} \quad (4.5)$$

The resulting temperature coefficient for thermionic emission, $(1/J_R)\partial J_R/\partial T$, is given by:

$$\frac{1}{J_R}\frac{\partial J_R}{\partial T} = \frac{1}{T}\left(\frac{q\Phi_{bn}}{kT}+2\right) = \alpha_T\ . \quad (4.6)$$

For a detector with a 0.36 eV Schottky potential, the temperature coefficient, $(1/J_R)\partial J_R/\partial T$, is 6%/K, at room temperature.

The mean square shot noise in the emission current is given by,

$$< i_{Shot}^2 >= 2qB_e A_e A_r T^2 e^{\frac{-q\phi_{bn}}{kT}} \quad (4.7)$$

where B_e is the electrical bandwidth of the detector read-out network.

The mean square Johnson noise in the detector is given by,

$$< i^2_{Johnson} >= \frac{4kTB_e}{r_{det}}, \tag{4.8}$$

where r_{det}, is the diode differential resistance,

$$\frac{1}{r_{det}} = A_e \frac{\partial J}{\partial V} = \frac{qA_e}{kT} J_S\, e^{qV/kT} \tag{4.9}$$

Consequently,

$$< i^2_{Johnson} >= 4qB_e A_e J_S e^{qV/kT}. \tag{4.10}$$

The detector is operated under a modest reverse bias, which is large compared to kT/q, so Johnson noise is generally negligible. In the absence of 1/f-noise, the total mean square electrical noise from the detector becomes:

$$< i^2_{Electrical} >=< i^2_{Johnson} > + < i^2_{Shot} >, \tag{4.11}$$

which can be expressed as:[21]

$$< i^2_{Electrical} >= 2qB_e J_R A_e \left(e^{qV/kT} + 1\right) \tag{4.12}$$

The detector output amplifier contributes additional noise[11]

$$< i^2_{amp} >= 2v^2_{na} \left(\frac{1}{R_f} + \frac{qA_e}{kT} J_s e^{qV/kT}\right)^2 \tag{4.13}$$

where v_{na} is the input referred voltage noise of the amplifier and R_f is the amplifier feedback resistance.

All of the above noise mechanisms are similar to mechanisms observed in photon detectors. Thermionic detectors will exhibit an additional noise, because of the low detector element mass. Thermal fluctuations in the detector will modulate the detector temperature and the related thermionic emission current. The contribution of thermal fluctuation noise to the mean square noise equivalent power (NEP) of the detector is given by:[22]

$$< NEP_{th} >^2 = 4kT^2 B_{th} G_{th}. \tag{4.14}$$

This noise will be observed as an additional electrical noise:

$$< i^2_{th} >= \frac{4kT^2}{C_{th}} \left(\frac{\partial I_s}{\partial T}\right)^2. \tag{4.15}$$

At any significant reverse bias above kT/q ($V_d > 100$mV), the diode impedance becomes very large, so as to give a negligible contribution to the amplifier noise. Under these conditions the total mean square noise becomes:

$$< i^2_{tot} >= 2qBA_e J_s + \frac{4kA_e^2 J_s^2}{C_{th}} \left(\frac{q\Phi_{bn}}{kT_b} + 2\right)^2 + 2\frac{v^2_{na}}{R^2_f} \tag{4.16}$$

5.0 NOISE EQUIVALENT TEMPERATURE FOR A THERMIONIC EMISSION DETECTOR

When a detector is illuminated by a source at ΔT_s, it will rise in temperature to ΔT_d, with a corresponding increase in diode current ΔI_d, given by:

$$\Delta I_d = I_d \alpha_T \Delta T_d = I_d \alpha_T H(T_s) \Delta T_s \tag{5.1}$$

where, α_T is the temperature coefficient for Schottky barrier thermionic emission, a electrical property independent of the detector thermal design, and $H(T_s)$ is the sensor thermal transfer function, given by Equation 3.23.

The signal to noise of this measurement is:

$$SNR_{th} = \frac{\Delta I_d}{\sqrt{< i_{tot}^2 >}} \tag{5.2}$$

and the Noise Equivalent Temperature is:

$$NEDT_{th} = \frac{\Delta T_s}{SNR_{th}} = \frac{\sqrt{< i_{tot}^2 >}}{I_d \alpha_T H(T_s)} \tag{5.3}$$

In an NEDT measurement ΔT_s is small. Therefore, $\xi(\Delta T_s)$ vanishes and Equation 5.3 becomes:

$$NEDT_{th} = \frac{(4F^2 + 1)(G_{rad} + G_{dif})\sqrt{< i_{tot}^2 >}}{I_d \alpha_T G_{rad} \Gamma(T_s, \lambda_1, \lambda_2) R(\tau_{th})} \tag{5.4}$$

6.0 NOISE EQUIVALENT TEMPERATURE FOR A PHOTOEMISSION DETECTOR

The blackbody response and NEDT for Schottky photo-detector arrays have been fully developed and will only be outlined here.[23, 24] The wavelength dependent quantum efficiency for photoemission is determined from Equation 2.2 as:

$$Y_\lambda = \frac{1.24 C_f}{\lambda}\left(1 - \frac{\lambda}{\lambda_c}\right)^2 \tag{6.1}$$

Where λ_c is the cut off wavelength, corresponding to the Schottky potential Φ_{ph}, as defined in Equation 2.4.

The spectral radiant emittance for internal photoelectrons, corresponding to Equation 3.16, is given by:

$$S_\lambda(\lambda, T_s) = 1.24 C_f \frac{2\pi c\left(1 - \frac{\lambda}{\lambda_c}\right)^2}{\lambda^5 \left(\exp\left(\frac{hc}{\lambda k T_s}\right) - 1\right)} \tag{6.2}$$

and the signal electrons collected per pixel is:

$$N_e(T_s) = \left(\frac{1}{4F^2 + 1}\right) A_e t_{fr} \int_{\lambda_1}^{\lambda_2} S(\lambda, T_s) d\lambda = N_{es} \tag{6.3}$$

The signal contrast at background temperature T_b, is:

$$\frac{1}{N_{eb}}\frac{dN_{eb}}{dT_b} = \frac{2hc}{(\lambda_1 + \lambda_2)kT_b^2} \tag{6.4}$$

We assume background noise limited operation. This is the usual case, for properly compensated thermal imaging photo-emissive arrays operating in the MWIR spectral band. Then, the mean square noise electron signal is:

$$< n_{eb}^2 >= N_{eb} \text{ (electrons)} \tag{6.5}$$

and the corresponding NEDT is

$$NEDT_{ph} = \frac{\sqrt{< n_{eb}^2 >}}{\left(\frac{dN_{eb}}{dT_b}\right)} \tag{6.6}$$

Using Equations 6.3, 6.4 and 6.5, The NEDT for photo-emissive detection is:

$$NEDT_{ph} = \left(\frac{(4F^2 + 1)}{A_e t_{fr} \int_{\lambda_1}^{\lambda_2} S(\lambda, T_b) d\lambda}\right)^{\frac{1}{2}} \frac{(\lambda_1 + \lambda_2)kT_b^2}{2hc} \tag{6.7}$$

7.0 COMPARISON OF INTERNAL EMISSION DETECTION MECHANISMS

In Table 1, we give the principal response functions for the Schottky barrier based photo emissive and thermal emissive infrared detection mechanisms. Note the "Response Functions" for the two detection mechanisms. The integral within ΔI_d for thermionic emission is the spectral radiant emittance.[25] The product of $1.24C_f$ and the integral within $N_e(T_s)$ gives the corresponding spectral radiant carrier emittance. Note the denominators of the two integrals are identical. The numerator terms show the flat spectral response for thermionic detection and the roll off with wavelength for photo-emissive detection. The roll-off is imposed by conservation of carrier momentum during emission and is the root cause of the low quantum efficiency of this detection process.

The thermionic emission response ΔI_d is reduced by the term

$$R(\tau_{th})/(G_{rad} + G_{dif}) \tag{7.1}$$

This term, the ratio of the detector roll off with frequency to the thermal conductance loss, is purely thermal. The thermal and electrical responses of the thermionic detector are separable and may be optimized independently. The thermal response alone determines the temperature rise ΔT_d of the detector element.

The electrical response is the thermodynamic equilibrium saturation current $I_s(T_d)$. The response can be optimized, by adjustment of the detector fill factor, bias voltage and Schottky potential, to increase $I_s(T_d)$, within the limits imposed by the focal plane read out network. Today, the principal response limitation thermal conductance to the focal plane substrate, G_{dif}, which is in the range, 3 to 5×10^{-8} watt/K. Reducing G_{dif} 10-fold will result in the response becoming background limited and a substantial increase in sensor signal to noise ratio. When G_{dif} is decreased thermal capacitance C_{th} must also be decreased, by reducing detector mass, to maintain sensor frequency response.

Table 1 **Comparative Response Functions for Photoemission and Thermionic Emission**

Parameter	Photoemission	Thermionic Emission
Response	$N_e(T_s) = \left(\frac{1.24}{4F^2+1}\right) C_f A_e t_{fr} \int_{\lambda_1}^{\lambda_2} \frac{2\pi c(1-\lambda/\lambda_c)^2 d\lambda}{\lambda^5(\exp(hc/\lambda k T_s)-1)}$	$\Delta I_d = I_d \frac{\Delta T_s}{T_b}\left(\frac{A_d \varepsilon_d R(\tau_{th})}{4F^2+1}\right)\left(\frac{q\Phi_{bn}}{kT_b}+2\right)\frac{\int_{\lambda_1}^{\lambda_2}\frac{2\pi hc^2 d\lambda}{\lambda^5(\exp(hc/\lambda k T_b)-1)}}{G_{rad}+G_{dif}}$
Primary Noise	$< n_{eb}^2 >= N_{eb}$	$< i_{tot}^2 >= 2qBA_e J_s + \frac{4kA_e^2 J_s^2}{C_{th}}\left(\frac{q\Phi_{bn}}{kT_b}+2\right)^2$
Response Time	$\tau_{ph} = R_d C_d$ $Y(h\nu)t_{fr}$	$\tau_{th} = \frac{A_d \rho c_d t_d}{G_{rad}+G_{dif}}$
NEDT	$NEDT_{ph} = \left(\frac{1}{N_e(T_b)}\right)^{1/2} \frac{(\lambda_1+\lambda_2)kT_b^2}{2hc}$	$NEDT_{th} = 2\sqrt{\frac{k}{C_{th}}}\frac{T_b(4F^2+1)(G_{rad}+G_{dif})}{A_d \varepsilon_d R(\tau_{th})\int_{\lambda_1}^{\lambda_2}\frac{2\pi hc^2 d\lambda}{\lambda^5(\exp(hc/\lambda k T_b)-1)}}$

Shot noise, from the infrared background signal, is the dominant noise in Schottky diode photo-emissive sensors. There are two noise comparable noise components in Schottky thermal emissive sensors, shot noise from diode saturation current and thermal fluctuation noise. As C_{th} is reduced to optimize sensor response, thermal fluctuation noise becomes dominant, until background limited performance is achieved.

Both detectors are based upon majority carrier emission, a process having response times below 0.1 nsec. Usually, the diode electronic response will be determined by the diode RC time constant. The practical response time for Schottky photo-emission sensors will be determined by the need to accumulate enough signal to give a useful SNR. This factor will be given by the product $N_e(T_s)$ x t_{fr}. Thermionic sensors will be limited by the thermal response time τ_{th}.

The photo-emissive NEDT equation is for infrared background limited operation and the thermal emissive NEDT equation is for thermal fluctuation noise limited operation.

In Table 2, we compare the theoretical response for two sensors based on photo emission and thermal emission. Both have 25 um pixels, equal electrical fill factors, and operate at f/1 and 60 frames per second. The thermal fill factor for the thermal emissive device is 0.90. We have assumed that both sensors have no optical losses and unity detector emissivity.

The NEDT predicted for photo-emissive sensors is in good agreement with the performance of a PtSi based sensor developed at AFRL in 1991. The AFRL camera had an f/2 cold shield. The measured camera NEDT was 0.062 K and the low frequency MRT was below 0.01 K. Schottky barrier based photo emissive sensors are fully developed and no significant improvement is expected for these devices.

The NEDT for thermal emission may seem high, but note that we have assumed a 60 Hz frame rate and a conductive loss of 50 nwatt/K. Given a state of the art loss of 30 nwatt/K, the NEDT would be reduced to 37 mK. In either case, at ranges up to 3 Km, we expect the LWIR thermionic emission sensor to have superior thermal imaging performance in field. In the MWIR band, solar reflection adds detail to the image, which obscures signals from objects having small temperature differences.

Table 2 Comparison of Photoemission and Thermionic Emission Thermal Imagers **F/1, 60 Hz frame rate cameras, with 25 um pixel dimensions**		
PARAMETER	PHOTOEMISSION	THERMIONIC EMISSION
Pixel / Fill Factor	25 um / 0.77	25 um / 0.90 / 0.77
Schottky Barrier Potential / C_f	0.22 eV / 0.30 $(eV)^{-1}$	0.33 eV / NA
Spectral Band	3.4 um - 5.2 um	8.0 um - 14 um
Operating Temperature	80 K	290 K
Radiation Conductance	NA	3.2Exp(-9) watt/K
Diffusion Conductance	NA	5.0 Exp(-8) watt/K
Diode Saturation Current	97 namp	27 uamp
Response for 1 K ΔT	25,000 electrons	4.8 namp
Dominant Noise	Background shot 5:1	Bias current shot 4:1
Total Noise	1,000 electrons	0.28 namp
NEDT	0.033 K	0.060 K (0.037 K at G_{dif+}=30 nwatt/K)

Thus, the solar image contributes clutter to the thermal imaging process, resulting in an increase in "effective NEDT" for fielded MWIR sensors.

We expect significant improvement in the response of Schottky barrier based thermal emissive sensors, as detector element mass is reduced and as thermal conduction losses are decreased. The projected improvement is shown in Figure 1. The shaded region on the right side of this figure indicates the current range of conduction losses, as given by G_{dif} reported for uncooled read out structures. When G_{dif} is reduced below 25 nwatt/K, the NEDT for thermionic emissive sensors will fall below the NEDT for the best photo emissive sensors. Although, as noted above, current art thermionic sensors, with higher NEDTs, may already give superior performance in the field.

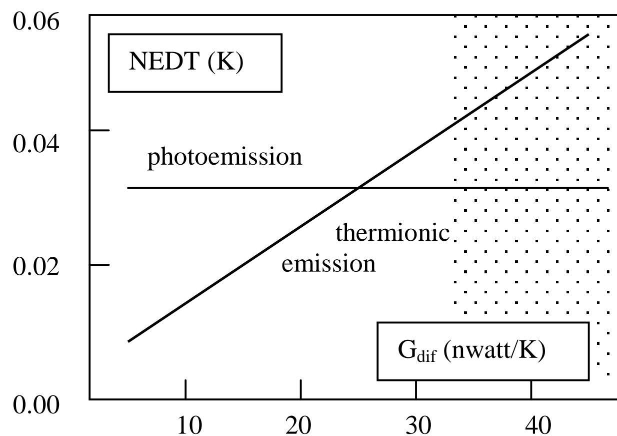

Fig. 1 Projected improvement of thermal emission sensor NEDT, with reduced thermal conductance.

8.0 Conclusion

We have derived the thermal imaging response functions for Schottky diode based photo emission and thermal emission sensors. We show Schottky diode based thermal emission sensors, based upon current array processing technology, have practical performance equal to the best Schottky barrier based photo-emissive sensors. We also show the potential for significant improvement of Schottky barrier based thermal emission sensors. We believe this technology could be used to

develop sensors with f/1 NEDTs below 10 mK. Thermal emission sensor arrays are fabricated using only silicon microcircuit processing. Thermal emissive devices have no detector 1/f-noise, although there may be 1/f noise in supporting read out circuitry. The use of thermionic emission detection will extend the use of uncooled silicon focal plane technology from the SWIR spectrum, near 1 um, to the LWIR spectrum, beyond 14 um.

---

[1] F. D. Shepherd and A. C. Yang, "Silicon Schottky Retinas for Infrared Imaging", Digest, International Electron Devices Meeting, pp. 310-313, 1973.

[2] G. A. Morton and S. V. Forgue, "An Infrared Pickup Tube", Proc. IRE, Vol. 47, pp. 1607-1609, 1959.

[3] J. O. Dimmock, "Capabilities and Limitations of Infrared Imaging Systems", Proc. SPIE, Vol. 32, pp. 9-23, 1972.

[4] J. A. Hall, "Problems of Infrared Television Camera Tubes vs Infrared Scanners", Appl. Optics, Vol. 10, pp.838-844, 1971.

[5] F. D. Shepherd, A. C. Yang, S. A. Roosild, J. H. Bloom, B. R. Capone, C. E. Ludington and R. W. Taylor, "Silicon Schottky Barrier Monolithic IRTV Focal Planes", Advances in Electronics and Electron Physics, Vol. 40B, Sixth Symposium on Photo-electronic Image Devices (Sept.1974), pp.981-992, 1976.

[6] J. M. Mooney, "Excess low-frequency noise in PtSi on p-type Si Schottky Diodes", IEEE Trans. Electron Devices, Vol. ED-38, pp. 160- 168, 1991.

[7] E. S. Kohn and M. L Schultz, "Charge-Coupled Scanned IR Imaging Sensors", AFCRL-TR-74-0375, 1974.

[8] W. F. Kosonocky, E. S. Kohn, F. V. Shallcross, D. J. Sauer, F. D. Shepherd, L. H. Skolnik, R. W. Taylor, B. J. Capone and S. A. Roosild, "Platinum-Silicide Schottky Barrier IR-CCD Image Sensor", Proc. 1978 International CCD Conference, Sec. 2, pp. 7-38, 1978.

[9] B. R. Capone, L. Skolnik, R. Taylor, F. D. Shepherd, S. Roosild and W. Ewing, "Evaluation of a Schottky Infrared Charge-Coupled Device (IR-CCD) Staring Mosaic Focal Plane", (See 26) Optical Engineering, Vol. 18, No. 5, pp. 535-541, September 1979.

[10] W. S. Ewing, "Silicide Array Compensation," Proc. SPIE, Vol. 409, Technical Issues in Infrared Detectors and Arrays, pp. 102-106, (1983).

[11] C. L. Kauffman, "Emergence of tactical framing infrared reconnaissance", Proc. SPIE, Vol. 3431, pp. 130-143, Airborne Reconnaissance XXII, Eds. W. G. Fishell, A. A. Andraitis, M. S. Fagan, J. D. Greer and M. C. Norton, November 1998.

[12] J. E. Murguia, P. K. Tedrow, F. D. Shepherd, D. Leahy, and M. M. Weeks, "Performance Analysis of a Thermionic Thermal Detector at 400K, 300K, and 200K", Proc. SPIE, Vol. 3698, Infrared Technology and Applications XXV, Eds. B. F. Andresen and M. S. Scholl, pp. 361-375, 1999.

[13] R. H. Fowler, "The Analysis of Photoelectric Sensitivity Curves for Clean Metals at Various Temperatures", Phys. Rev., Vol. 38, pp. 45–57, (1931).

[14] C. R. Crowell, W. G. Spitzer, L. E. Howarth and E. E. Labate, Attenuation Length Measurements of Hot Electrons in Metal Films", Phys. Rev., Vol. 127, 2006, (1962).

[15] R. Williams, "Injection by internal photoemission," Semiconductors and Semimetals, Vol. 6, Academic Press, New York, NY, pp. 97-139, 1970.

[16] J. M. Mooney and J. Silverman, "The Theory of Hot-Electron Photoemission in Schottky-Barrier IR Detectors," IEEE Trans. on Electron Devices, Vol. ED-32, No. 1, January 1985.

[17] R. J. Archer and J. Cohen, "Schottky Barrier Monolithic Detector Having an Ultra-thin Metal Layer," U. S. Patent No. 3,757,123, Sept. 1973.

[18] J. M. Mooney, "Infrared optical absorption of thin PtSi films, 1 and 6 um," J. Appl. Phys. Vol. 64, pp. 4664-4667, 1988.

[19] Murguia and Tedrow, et al, Ibid. 1999.

[20] S. M. Sze, Physics of Semiconductor Devices, Chapter 5, John Wiley & Sons, 1981.

[21] S. M. Sze, Ibid. pp. 130-131.

[22] B. R. Johnson, P. W. Kruse, "Silicon Microstructure Super-conducting Microbolometer Infrared Arrays," Proc. SPIE 2020, Infrared Technology XIX, B. F. Andresen and F. D. Shepherd, Editors, 2-11, 1993.

[23] F. D. Shepherd and A. C. Yang, et al, Ibid. 1976.

[24] F. D. Shepherd and J. M. Mooney, Design considerations for IR staring mode sensors", Proc. SPIE, Vol. 762, Electro-Optical Imaging Systems Integration, pp. 35-50, April 1987.

[25] J. M. Lloyd, Thermal Imaging Systems, Plenum Press, New York and London, p.20, 1975.